Supporting information

# $W_{18}O_{49}$/N-doped reduced graphene oxide hybrid architectures for full-spectrum photocatalytic degradation of organic contaminants in water

*Jia Wang,[a#] Xiaochen Fang,[a,b#] Yue Liu,[a] Ming-Peng Zhuo,[a,b]* Mu-Dan Yao,[a] Su-Lei Fu,[c] Zuoshan Wang,[d]* Weifan Chen,[a]* Liang-Sheng Liao[b]*

[a] School of Materials Science & Engineering, Nanchang University, Nanchang, Jiangxi 330031, China.

[b] Jiangsu Key Laboratory for Carbon-Based Functional Materials & Devices, Institute of Functional Nano & Soft Materials (FUNSOM), Soochow University, Suzhou, Jiangsu 215123, China

[c] Key Laboratory of Advanced Materials (MOE), School of Materials Science and Engineering, Tsinghua University, Beijing 100084, China

[d] College of Chemistry, Chemical Engineering and Materials Science,Soochow University, Suzhou, Jiangsu 215123, China.

Authors to whom correspondence should be addressed: chenweifan@ncu.edu.cn (W. F. Chen); mpzhuo@suda.edu.cn (M. P. Zhuo); zuoshanwang@suda.edu.cn (Z. S. Wang).

#These authors contributed equally to this work.

## Experimental details

### Materials

All the chemicals are analytical grade and can be used without further purification, including crystalline flake graphite (C), hydrochloric acid (HCl), sulfuric acid ($H_2SO_4$), sodium nitrate ($NaNO_3$), potassium permanganate ($KMnO_4$), hydrogen peroxide solution ($H_2O_2$), ammonium nitrate ($NH_4NO_3$), glycine ($C_2H_5NO_2$), ammonium metatungstate [$(NH_4)_6H_2W_{12}O_{40}\cdot H_2O$, AMT] and rhodamine B (RhB). Dialysis bags were used during the synthesis process of graphene oxide.

### Measurements

The phase composition of the samples will be analyzed by X-ray diffractometer (XRD, Bruker D8 Advance) with Cu Kα radiation (λ=0.154 05 nm). The morphologies of different samples were characterized on a field emission scanning electron microscopy (SEM, FEI Quanta200F). The microstructures of the samples were observed by transmission electron microscopy (TEM, JEOL JEM-2100). The elemental composition of the sample surface and the W4f binding energy were determined by X-ray photoelectron spectroscopy (XPS). On the other hand, the ζ potential of the sample with 250 mg/L concentration was measured by a Malvern Zetasizer instrument (Nano S90, Malvern Instruments Ltd.) at 30 °C. The photocurrent of the samples under UV, Vis and NIR were recorded at a basic of 0 V versus the reference electrode, which could be obtained by an electrochemical workstation. During the test process, an ITO glass coated with $W_{18}O_{49}$/N-rGO was used as working electrode, the Pt and $Na_2SO_4$ solution (0.5 mol/L) were acted as reference electrode and electrolyte respectively. The photoluminescence property of products was evaluated by fluorescence spectrometer (FLS 1000) with an excitation wavelength of 270 nm and a scanning wavelength range of 300-800 nm.

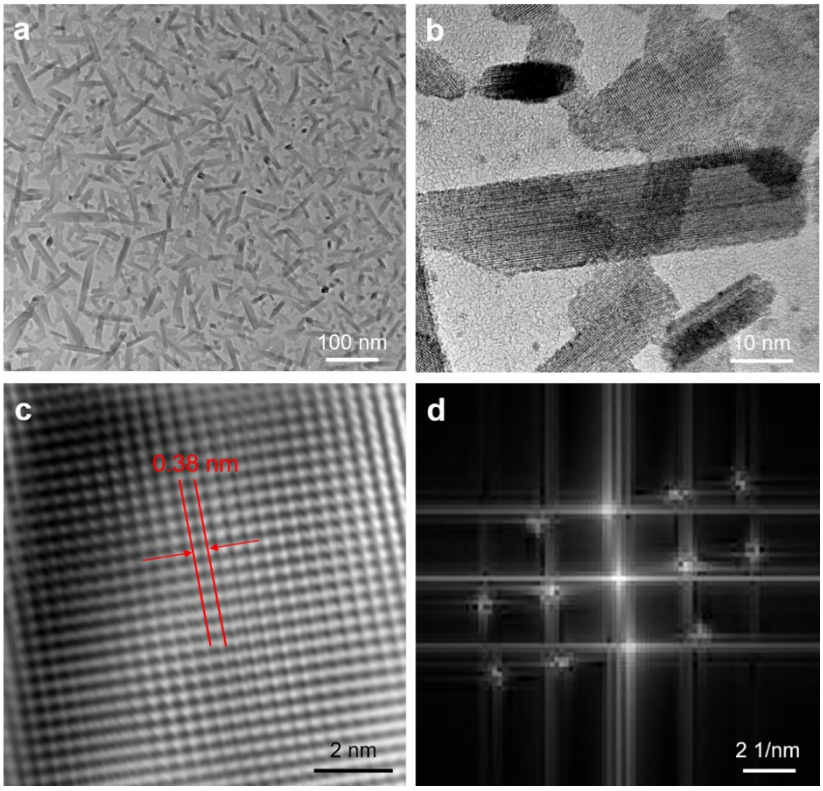


**Figure S1.** (a) The low-magnification TEM image of the as-prepared $W_{18}O_{49}$. (b) The high-magnification TEM image of the as-prepared $W_{18}O_{49}$/N-rGO. (c) The HRTEM image of one typical $W_{18}O_{49}$ with the scale bar of 2 nm. (d) The corresponding SAED of $W_{18}O_{49}$ in (c).

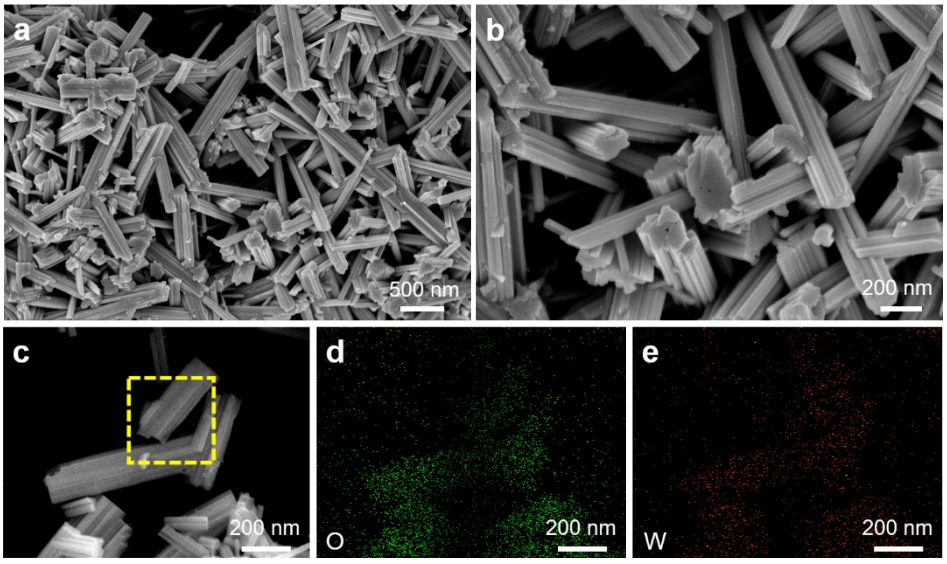


**Figure S2.** The SEM images (a-c) and Energy-dispersive x-ray spectroscopy (EDS) mappings of (d) O, and (e) W of synthesized $W_{18}O_{49}$.

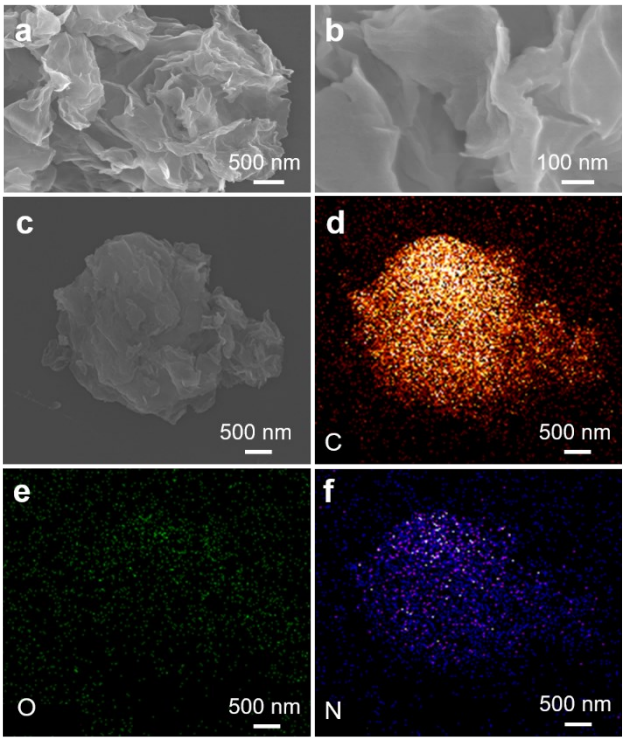


**Figure S3. T**he SEM images (a-c) and the EDS mappings of (d) C, (e) O, (f) N of synthesized N-rGO.

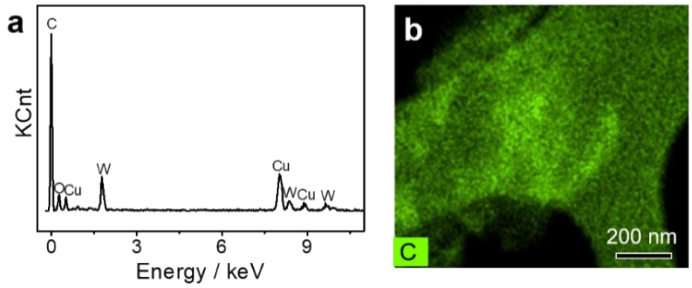


**Figure S4.** (a) The EDX spectrum of $W_{18}O_{49}$/N-rGO. (b) The elemental mapping (C element) of $W_{18}O_{49}$/N-rGO.

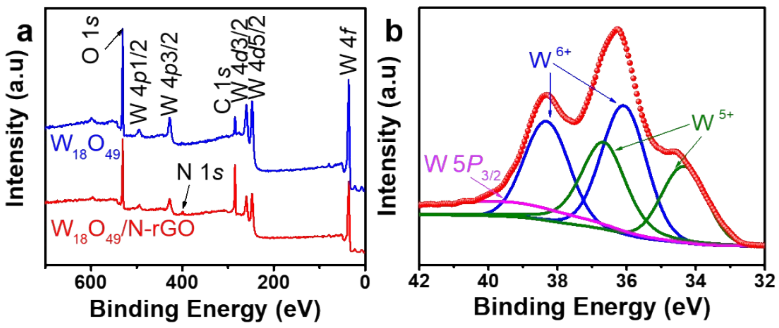


**Figure S5.** (a) Full range XPS spectra of $W_{18}O_{49}$ and $W_{18}O_{49}$/N-rGO. (b) The W4f core level XPS spectra of $W_{18}O_{49}$.

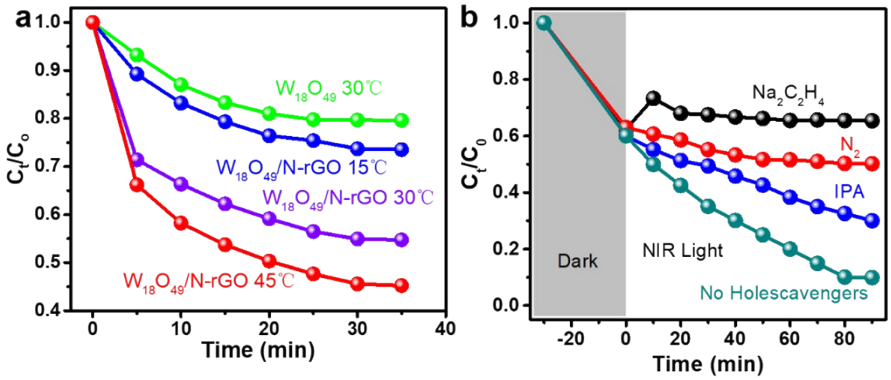


**Figure S6.** (a) The time-dependent adsorption curve of RhB degraded by the $W_{18}O_{49}$/N-rGO at different temperature of 15, 30 and 45 °C, and that of the $W_{18}O_{49}$ sample at 30 °C. (b) The effects of different active species scavengers on the degradation rate of RhB by $W_{18}O_{49}$/N-rGO under NIR irradiation.

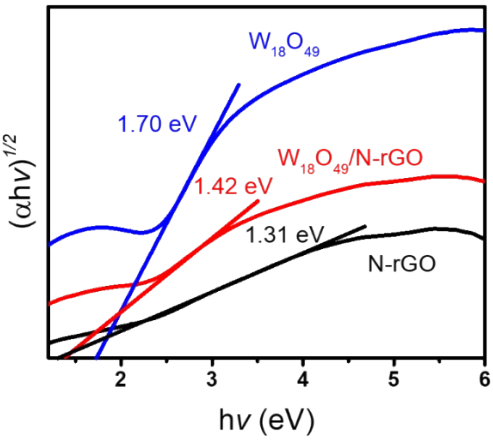


**Figure S7.** Tauc plots [$(\alpha hv)^{1/2}$ vs. $hv$] of N-rGO, $W_{18}O_{49}$ and $W_{18}O_{49}$/N-rGO.

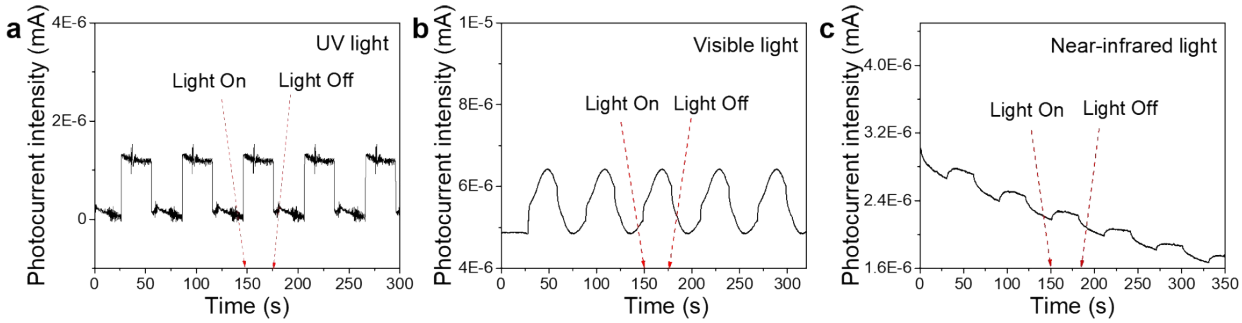


**Figure S8.** The photocurrent response of $W_{18}O_{49}$/N-rGO under UV light (a), Visible light (b), and Near-infrared light (c).

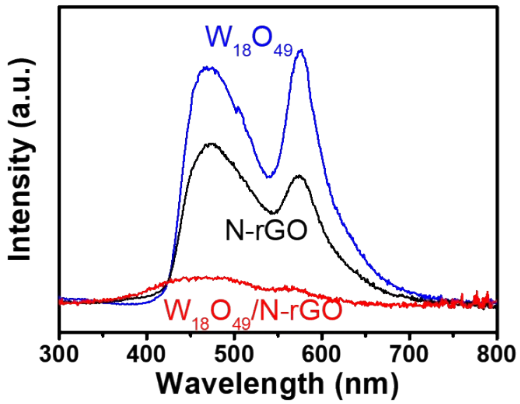


**Figure S9.** Photoluminescence spectrum of N-rGO (black line), $W_{18}O_{49}$ nanorods (blue line) and $W_{18}O_{49}$/N-rGO hybrid nanomaterials (red line) with the excitation wavelength of 270 nm.